When a fluid-structure interaction keeps you awake: a physical approach to Obstructive Sleep Apnea

A. Van Hirtum[1], F. Chouly[1,2], P.Y. Lagrée[3], J.R. Paoli[4], Y. Payan[2], X. Pelorson[1]

je vais faire [1]ICP, CNRS UMR 5009 - Institut National Polytechnique de Grenoble, Grenoble, France
[2]TIMC, CNRS UMR 5525 - Université Joseph Fourier, La Tronche, France
[3]LMM, CNRS UMR 7607 - Université Paris 6, Paris, France
[4]CHU Purpan, Toulouse, France

Abstract

The Sleep Apnea Syndrome is known to be related with a partial (hypopnea) or total (apnea) collapse of the upper airway. The patency of the upper airway is dictated by a combination of passive mechanical properties and active neural mechanisms. From a physical point of view, neglecting active neural control mechanisms, the airway collapse can be explained by the interaction of the airflow during respiration (fluid) with the surrounding tissues (structure). The characteristic recurrent collapse causes about 3 % of the adult population to suffer from Obstructive Sleep Apnea (OSA). A systematic review of published studies on OSA insists on the necessity of a better understanding of the factors determining the airway obstruction in order to improve modelling, simulation and eventually prediction of the fluid-structure interaction at the origin of OSA. Prediction of OSA is in particular important to foresee the outcome of surgical procedures and to estimate its long-term effectiveness. In order to be of practical use a surgical prediction tool demands reliable and accurate simulation results available within a reasonable time delay and exploiting relevant and 'in-vivo' accessible physiological data. In order to contribute to the understanding of OSA a physical approach is presented consisting mainly of three stages. At first, relevant physical quantities are formulated based on physiological 'in-vivo' observations in order to define the problem. Secondly, a simplified theoretical model is proposed based on assumptions derived of the order of magnitudes derived during the first stage. Thirdly, an experimental validation of the assumptions and of the accuracy of the theoretical model is performed in a suitable experimental setup allowing to control model input parameters and to measure model output parameters.

1 Obstructive Sleep Apnea: a nowadays health issue

Sleep apnea has been divided classically into two forms: Obstructive Sleep Apnea (OSA), in which partial (hypopnea) or total (apnea) collapse of the upper airway results in

decreased airflow despite continued respiratory effort, and central sleep apnea, in which decreased airflow results from reduced respiratory effort.
The Obstructive Sleep Apnea Syndrome is defined as repeated episodes of obstructive hypopnea and apnea during sleep and is manifested by the intermittent decrease or cessation of breathing [40, 106]. OSA has been extensively shown to be an important health care issue affecting all stages of life with a reported prevalence of 2 % in childhood, 2 to 4 % in middle-aged adults and more than 10 % of the population over the age of 65 [5, 30, 81, 117]. Therefore although originally seen as a minor health issue anecdotically treated as the Pickwick syndrome to a character in Dickens 'Papers of the Pickwick Club' resembling at the classic obese, sleepy OSA patient [15] during the last 20 years OSA has earned the doubtful reputation of the most common disorder of breathing during sleep.
Except preventing the pleasure of a good night of sleep, patients chronically suffer the consequences of repeated sleep disruption as well as recurrent hypoxaemia and hypercapnia [36, 81]. Therefore OSA is a chronic disorder causing excessive daily sleepiness and increasing the development of cardiovascular diseases and arterial hypertension [80, 87, 116]. Consequently, OSA has adverse and processing consequences on the patient's daily life, is associated with an increased risk of public traffic accidents to seven times that of the general driving population and increases the risk of morbidity and mortality due to cardiovascular and cebrovascular causes [31,34,52,72,80,81,106,108,115].

2 Pathogenesis of OSA

The upper airway is a potentially collapsible structure. The pathogenesis of OSA is characterised by recurrent collapse in the upper airway. The narrowing or closure may occur at one or more sites in the upper airway between the tip of the soft palate to the glottal inlet, i.e. in the velopharynx, oropharynx and hypopharynx [1, 5, 8, 19, 27, 36, 79, 91, 98, 112]. The patency of the upper airway is dictated by a combination of passive mechanical properties and active neural mechanisms. Therefore specific sites of narrowing or closure are influenced by among others the underlying neuromuscular tone, upper airway muscle synchrony, stage of sleep, soft-tissue, skeletal and craniofacial factors determining the upper-airway size, length and recurrent vibratory trauma (snoring) of the soft palate [8, 26, 36, 54, 56, 62, 72, 81, 106, 107]. Moreover, dynamic observations strongly suggest that regardless of the origin of the collapse, eventually the entire pharyngeal segment of the upper airway may be involved [1, 5, 91, 93]. Expiratory narrowing is reported to produce a significant reduction of retropalatal airway cross-sectional area at end-expiration prior to obstructive apnea [79]. The size of the upper airway is the smallest during sleep, at the end of expiration. Upper-airway resistance increased earlier during expiration prior to changes occurring during inspiration [107]. This finding suggested an important role of the expiratory phase in promoting upper-airway collapse and is related to the inspiratory instability occurring when lowering the expiratory pressure in patients with OSA. So, the upper

airway collapse is found to initiate in the oropharynx, processing to the hypopharynx and involves both inspiration as expiration since increased collapse on expiration predisposes a mechanism for increased obstruction on subsequent inspiratory breaths [79, 107, 111].

3 Diagnosis, treatment, understanding: an open story

'Of all sciences Physiology is most exposed to causes of inaccuracy. The subjects of experiment are here the most complicated, and the phenomea at once the most varied, and bearing the least resemblance to those we are accustomed to contemplate [89].'

OSA is not different and questions arising from medical literature concerning diagnosis, treatment and understanding are multiple stressing the need for further understanding and a physical theoretical and experimental modelling of OSA.

3.1 Diagnosis and follow-up of OSA . . .

Monitoring tools has been developed to assess likelihood of OSA for use either inside (in-laboratory polysomnography) or outside the hospital (at home). These include simple questionnaires about symptoms as well as the recording of multiple variables during sleep incorporating among others airflow, electroencephalogram (EEG), electro-oculogram, snoring (microphone), the movements of the rib cage and of the abdomen and oxygen saturation [25, 29, 42, 73, 81, 86, 88, 90, 92, 105–107]. In particular for ambulatory studies the reported results of specialized devices might be associated with multiple causes and currently evidence to support use of these newer technologies for diagnosis in routine clinical practice is lacking. This is not because of inadequacy of the technology per se but rather the quality of studies to assess the effectiveness of these alternative strategies. In general it can be said that there is a rapidly growing demand for diagnosis and treatment of OSA since knowledge taken for granted is reput into question. Recent data indicate that the relation between sleep apnea and diurnal hypertension is independent of obesity, age and sex and so the original simplified view of astute physicians of the Pickwickian syndrome needs revision. In particular the found interaction between central and obstructive sleep apnea might require new insights both for diagnosis as for treatment as will be pointed out in the next section [39, 81, 106]. Since as the understanding of the pathophysiology of sleep apnea has increased, however, the dichotomy between central and obstructive sleep apnea has become less clear.
So, diagnosis and follow-up of OSA . . . benefits from increased understanding, in particular explaining the cause symptom relationship.

3.2 Treatment of OSA ...

The obstructive sleep apnea syndrome (OSAS) is mainly treated using empirical therapeutic procedures. Therapeutic strategies for patients with sleep apnea may be grouped into three general categories: behavioral, medical and surgical [106]. Firstly, behaviour therapy aims to inform patients on risk factors increasing the severity of upper-airway obstruction such as the use of alcohol, sedatives, sleep position and increased weight. Secondly, medical therapies consists mainly in continuous positive airway pressure and pharyngeal appliances. Long-term use of medical therapeutic treatment strategies, such as continuous positive airway pressure or pharyngeal appliances, causes daily discomfort and reduces the quality of life [33]. Furthermore as noted in the previous section the use of medication is although currently disappointing a promising perspective for the future exploiting the interaction of central and obstructive sleep apnea [39, 97]. Thirdly, surgical procedures are available for patients with severe apnea who cannot tolerate positive pressure. The long-term effectiveness of surgical treatment is estimated to range between 50 and 78 %, depending on the surgical procedure applied and consequently does not guarantee uniform success [13, 23, 33, 66, 73, 81, 101, 103, 106]. Therefore current research aims to improve the diagnosis, follow-up and treatment of OSA. In particular, the need for further understanding of the OSA syndrome to favour successful development of therapeutic and surgical treatments is stressed [8, 33, 52, 67, 78, 83, 86, 91]. Even as the understanding of the interaction between anatomic and neuromuscular factors in the pathogenesis of sleep apnea increases, it is likely that modifications of neuromuscular factors will play a useful therapeutic role [30, 39, 81]. In the meantime, treatments that primarily modify airway anatomy during sleep (e.g. CPAP, surgery and oral appliances) will probably remain the most important tools in the treatment of sleep apnea although not generally tolerated and not uniform successful [39, 81].
So, treatment of OSA ... benefits from increased understanding enabling among others surgical prediction.

3.3 Underlying mechanism of OSA ...

During wakefulness, the patency of the upper airway is under both volitional and nonvolitional control. However, during sleep, pharyngeal patency is almost exclusively under nonvolitional control. Even though it is clear that the airway collapses in patients with sleep apnea, the precise mechanism is unknown. Because of the complicated arrangement of the muscles as well as the varying sleep states, it has not been possible to precisely define whether the collapse is due primary to altered neural or mechanical control, or a combination of both factors. Moreover, the ability to dissect out the relative contribution of neuromuscular activity and the contraction and/or relaxation of various muscles has been hampered by the inability to develop a biomechanical model that could determine the relative influences of the various factors causing collapse [80]. Models providing physical

insight in OSA occurrences should allow to reconsider quotations like, e.g. *anatomic narrowing of the upper airway due to obesity or craniofacial morphology is a consistent feature for OSA* [39] or *OSA in which collapse of the upper airway results in decreased airflow despite continued respiratory effort* or *as the severity of obstructive sleep apnea increases, airway collapse occurs with less extreme negative pressure, reflecting greater anatomic compromise of the upper airway* or *a decrease in the pharyngeal transmural pressure alone is a sufficient condition for the production of the sleep apnea syndrome in normal individuals* [56] or *who with sleep apnea will benefit from therapy* [81], in terms of a physical model outcome and parameters. At longterm expressions commonly retrieved in medical literature as *critical narrowing* [20], *critical closing pressures*, *the upper airways behave as predicted by the Starling resistor model* [8, 56, 62, 68], *balance of forces model* [81], *extraluminal tissue pressure: what does it mean ?* [100], *Why does one snores ? What are the conditions required for snoring ?* [6] should be objectively (re)-evaluated and eventually quantified. Moreover a purely mechanical explanation might contribute to the understanding of the interaction between anatomic and neuromuscular factors by means of elimination of the latter in the physical model.
So, the underlying mechanism of OSA ... needs to be cleared out in terms of principal phenomena involved.

4 A challenge: physical OSA pathogenesis

A growing number of reports in literature demonstrate an ongoing commitment among scientists and physicians to improve our understanding of sleep-disordered breathing [66]. The present study is a contribution to the development of physical theoretical and experimental models for OSA towards the definition of physical OSA pathogenesis.
From a physical point of view, neglecting neural mechanisms, the airway collapse is due to the fluid-mechanical interaction of the fluid (airflow during respiration) and the surrounding structure (tissues). Studies of the biomechanical pharyngeal airflow and resulting pressure distribution or forces in cases of OSA are very limited. Because of a wide clinical interest, most of the literature in the field concentrates on the relationship between inspiratory and expiratory pressure and the volume flow velocity. In the following existing models are reviewed evolving from classical models to current model approaches. Different modelling issues are discussed in particular with respect to the ongoing flow phenomena. Finally a methodology to model the fluid-structure interactions is proposed in particular aiming to predict the long-term effectiveness of surgical interventions.

5 Physical models with respect to OSA

Breathing is clearly related to the study of time varying physical quantities as volume flow velocity, pressure difference, pressure distribution in an airflow channel consisting of the upper airways. In a clinical context the variables of interest are assessed in numerous studies and generally presented as a pressure-flow relationship representing the volume flow produced in response to a respiratory effort.

5.1 Mathematical fitting of the pressure-flow relationship

Usually, the pressure-flow relationship [14, 53, 104, 107] in the upper airway is mathematically fitted by a quadratic or polynomial function so as objectively to detect inspiratory flow limitation and related phenomena [44, 74]. The resulting pressure-flow relationship obtained by curve fitting of the applied mathematical polynomial or quadratic formulation may provide useful empirical information, but does not describe the complexity of the ongoing physical flow behaviour and does not inform on the pharyngeal pressure distribution even if the obtained coefficients can be associated with the relative importance of different terms in a simplified volume flow description [74]. The interaction between the fluid and the surrounding upper airway tissue is expressed by the force exerted by the fluid on the surrounding tissue. This force is determined by the pressure distribution. Therefore, not only does the volume flow velocity need to be accurately predicted from the upstream pressure, as was the aim in [44] and [74], but also the pressure distribution along the upper airway. With respect to an accurate description of the pressure distribution, it is generally accepted that an accurate prediction of flow separation is crucial [76, 84].
The next in this line of enquiry present themselves as a clear-cut challenge: to develop theoretically the characteristic pressure-flow relationships from basic physical principles [14] as well as to predict the pressure distribution.

5.2 Classical models

Currently in medical literature there are mainly two models that for OSA have been put forth, i.e. the balance of forces model and the Starling resistor model, respectively [36, 80].

5.2.1 Balance of forces model

Since the original physiological description of airway collapse, it has been proposed that the upper airway patency is determined by the balance between the negative intraluminal airway pressure (airway suction) and the dilator muscle tone. This is called the *balance of forces model* in which negative intraluminal pressure is promoting collapse of the airway

with activation of airway dilator muscles promoting patency, the net effect during wakefulness is for patency [81]. Remmers and others [93] noted a demonstrable fall in phasic genioglossus activation at the onset of the apneas and suggested that an inappropriately low level of activity did not counterbalance the collapsing force exerted by the respiratory pump muscles. Various inputs including the peripheral and central chemoreceptors as well as other factors that increase neural input to either the diaphragm (inspiratory drive) or upper airway muscles (upper airway drive) will be important in determining upper airway patency. However the model allows not to quantify the forces generated by the specific dilator muscles relative to the negative intraluminal pressure.

5.2.2 Starling resistor analogy

The Starling resistor is a classical experiment used to study biofluid mechanical applications involving collapsible structures, such as flow limitation in the airway branches and blood flow [8, 14, 21, 22, 41, 55, 57, 60, 68, 71, 80, 104]. It thanks its popularity to qualitative agreement with experimental tests although quantitative agreement is not always provided. This model views the structures of interest as collapsible tubes. Their behavior is characterized by a flow pattern which initially increases as driving pressure increases; however, above a critical driving pressure, there is a progressive plateauing of flow at some maximal level despite continued increase in driving pressure (flow limitation). One can study this behavior mathematically, or demonstrate it with a physical model consisting of a thin walled elastic (collapsible) tube enclosed in a chamber. The pressure in the chamber (Pcrit) can be varied to be less than or greater than the pressure inside the tube. The analysis of such a system predicts that maximal flow through the tube segment is determined by two separate factors: the resistance of the upstream segment (e.g. at nose) and the transmural pressure surrounding the collapsible segment. This corresponds to a 'tissue pressure' in the collapsible parts of the upper airway. When Pcrit is greater than 0, there is airway collapse at rest and obstruction of the tube occurs. When Pcrit is strongly negative, the airway will remain patent even under large inspiratory efforts. There is strong evidence that the hypotonic pharyngeal airway behaves like a Starling resistor. In normal subjects a negative Pcrit has been measured, whereas in snorers Pcrit approaches 0 and in obstructive apnea patients, Pcrit may be positive [8]. However, it must be emphasized that this description of the airway refers to the passive airway, i.e. without added muscle activity that cannot easily be measured during normal breathing. To further model the airway in the intact human beyond its passive properties, one must add the effects of upstream resistance (anatomy) and changes in collapsibility mediated by changes in baseline and phasic muscle tone. At submaximal flows, increasing upper airway muscle tone has been shown to result in decreasing resistance. However, at maximal flow, increasing upper airway tone (activation) changes the value of Pcrit for a Starling resistor. This causes an increase in the maximum flow through the Starling resistor by decreasing airway collapsibility of the flow-limiting segment [54] and can occur even without a change in the resistance (i.e. both flow and pressure can increase). Thus the Starling model helps to characterize the changes in flow that

occur with changes in muscle tone. Total collapse and cessation of flow never was observed in the Starling resistor model by e.g. [22,55,57,60] and self-sustained oscillations or flutter are prominent [10]. The pressure drop over the length of the tube is described as a function of the flow and the quantity external pressure minus downstream or upstream pressure. However, collapsible tube models are far from realistic simulations of the collapse in the upper airway. The human pharynx is far from an axisymmetric tube not only in his geometrical structure (rigid hard palate against soft tissues), but also in the mechanical properties of the surrounding tissues [49]. Owing to the pharyngeal asymmetry in both geometry and tissue properties, the relevance of such devices for the study of OSA is not obvious and considering an alternative model is motivated.

5.3 Lumped segments models

Several simplified mathematical models of the collapsible upper airway are presented in literature exploiting one, two or multiple lumped collapsible segments [2, 7, 35, 38, 48–50, 111]. The approach is of interest since it allows at least qualitatively to describe a rich mechanical behaviour including collapse and flutter. Critical conditions for occlusion can be defined starting from rude approximations of anatomical and physiological properties. Furthermore simplified lumped models allows to evaluate the relative importance of several physical phenomena like viscosity in the flow model [35,94,109]. Multiple elements might represent different collapsible sites or differences in physiological properties. Moreover due to the simplifications physiological properties can be related to a limited amount of model parameters. This feature can be exploited to link the proposed mechanical model to more general control models for muscle activation or respiratory modelling as e.g. presented for the genioglottal activation during sleep [46, 49, 50, 62] or a one-dimensional flow model accounting for the chemoreceptor feedback for carbon dioxide concentration in the brain stem [3]. However the unrealistic assumptions and physiological simplifications do not allow to yield the quantitative precision necessary in e.g. tools aiming to predict surgical outcome. Besides, the determination of the required model parameters on 'in-vivo' subjects is far from solved and is a major drawback for clinical applications of lumped segments models.

5.4 Flexible beam models

Snoring receives a great deal of attention from a medical point of view among others because of its possible relationship with OSA [72]. Except the mentioned lumped models described in [2, 38] a biomechanical model of the soft palate is obtained by modelling the flexible structure as a continuous beam [6,9,47,70]. Although the presented model outcome is very interesting for understanding the onset of instability the models are limited. Firstly because of the obvious geometrical limitation to the soft palate and secondly due to the fact

that snoring although often related is not necessarily a consequence of OSA and even if related snoring is more a consequence as a cause.

5.5 Numerical modelling

A three-dimensional computational simulation of airflow characteristics, including both volume flow velocity and pressure distribution, in an anatomically accurate rigid human pharynx geometry is assessed in [102]. The airflow was assumed to be incompressible and steady. The pressure drop in the pharynx was quantified to lie in the range of 200-500 Pa, provoking the pharynx to collapse. The switch from laminar to turbulence was found to increase the pressure drop by 40 %. Subtle effects on the airway morphology, as introduced by surgical treatment of OSA, where shown to have a great effect on the pressure drop. More recently [4,69,113,114] image-based CFD is applied to study the effect of airway geometry on upper airway pressure and flow resistance in children with sleep apnea. In [113, 114] an experimental study using a scaled rigid model validated the CFD predictions. Due to the large computation time exceeding 10 hours [113, 114] propose to exploit CFD models as a benchmark firstly for building simplified models of pressure drop in the pharynx in order to analyze larger number of subjects and secondly for incorporation into dynamic system models. In this framework [4] propose to apply extremely simplifying scaling factors to the proposed CFD model in order to extrapolate between subjects characteristics including adults. Without arguing the quality and the interest of the mentioned studies, it should be noticed that the approximations of rigid structures and steady flow conditions are severe simplifications due to the complex and dynamic nature of OSA involving deformable structures and unsteady flow. Three-dimensional numerical modelling of a collapsible segment is presented in e.g. [75] for the Starling resistor analogy and therefore not considered here.

6 Motivation for further physical OSA modelling

The previous section illustrates both the relevance and limitations of physical theoretical and experimental models for OSA found in literature. In particular with respect to clinical application and surgical planning the necessity of further research is put forward. The reasons are multiple depending on the applied model approach. Firstly, simplifying theoretical models predispose understanding of the basic mechanisms, but lack precision in e.g. the anatomical description necessary for clinical applications. Moreover matching simplified models to the complexity of individual subject characteristics can hardly be accomplished. Secondly, accurate numerical models require a lot of computational capacity and demand a calculation time which is to long to fit into a clinical practice. Besides computational loads the presented numerical models exploit in general rigid static geometries incapable of representing the dynamical features of OSA and hence the full complexity of the fluid-structure interaction. Thirdly the classical Starling experimental model of a collapsible tube

does not represent the reality of OSA and hence alternative experimental models for theoretical model validation should be assessed. Finally and most importantly much of the phenomena occurring during a single collapse event are still subject to current research for both the experimental and the theoretical modelling, respectively. Current issues with respect to the collapsible tube are e.g. presented in [11, 82]. Recent research with respect to e.g. impact, movement, antisymmetry in fluid-structure interaction modelling is described in among others [37, 51, 59, 61, 64, 65].
It seems that considering 1) the current state of the art in physical modelling both from a theoretical as an experimental point of view, 2) the state of the art in physiological understanding of the OSA syndrome as well as 3) considering the need in clinical practice for e.g. a surgical prediction tool a compromise between complexity and accuracy is opportune.
In the following theoretical models simplifying the ongoing physiological and physical complex reality are proposed as well as an experimental approach in order to validate the underlying assumptions and to study specific modelling issues in a controlled, measurable and reproducible way. The presented research aims to contribute to the understanding of flow-induced pharyngeal airway obstruction at the origin of OSA.

7 Towards an accurate simplified physical flow model

The presented physical approach consists mainly of three stages. Firstly, the formulation of relevant physical quantities based on 'in-vivo' physiological data in order to define the problem. This crucial stage at the basis of the theoretical model formulation, stresses the importance of an interdisciplinary approach. Secondly, a simplified model is proposed based on assumptions derived of the obtained quantities during the first stage. Thirdly, an experimental validation of the proposed theoretical model is performed in a suitable experimental setup allowing to control model input parameters and to measure the model outcome.

7.1 Assumptions and dimensional numbers

From a fluid mechanical point of view several flow assumptions can be formulated on the basis of a dimensional analysis of the governing flow equations. This yields a set of non-dimensional numbers, which can be interpreted as a measure of the importance of various flow effects. Based on the obtained orders of magnitude for the characteristic non-dimensional numbers approximations are made to describe the flow. Concerning obstructive sleep apnea four non-dimensional numbers are derived based on characteristic conditions listed in Table 7.1. Physiological data are obtained from 'in-vivo' observations [63, 77, 80, 99].
Firstly, the squared value of the Mach number, $Ma = \frac{U_0}{c_0}$, the ratio of flow velocity U_0 to the speed of sound c_0 indicates the tendency of the flow to compress as its encounters

L_0	tongue length	5 cm
W_0	pharyngeal width	3 cm
h_0	minimum aperture	2 mm
c_0	speed of sound	350 m.s^{-1}
ρ_0	mean density	1.2 kg.m^{-3}
μ_0	dynamic viscosity	1.5 10^{-5} $m^2.s^{-1}$
t_0	period of breathing (inspiratory)	4 s
U_0	flow velocity(*)	8 m.s^{-1}

Table 1: Characteristic conditions during obstructive sleep apnea. (*) Estimated from typical volume flow velocity of 30 l.min^{-1}.

a solid boundary. Since the velocities involved during respiration are small compared with the speed of sound in air ($Ma_0^2 \approx O(10^{-4})$) the flow is assumed to be incompressible.
Secondly, the Strouhal number $Sr = \frac{L_0}{t_0 U_0}$, is a dimensionless frequency indicating the ratio of the distance over which flow is convected in a characteristic time t_0 over a characteristic width L_0 of a structure exposed to the flow. The airflow can be considered as primarily steady as long as the flow patterns at any given time are approximately the same, which is reasonable during quiet breathing at the characteristic respiratory frequencies and rigid walls expressed by a low Strouhal number $Sr_0 \approx O(10^{-3})$.
The assumptions of incompressible and steady flow will not be discussed in the present chapter. The assumptions are indeed widely accepted in literature [41, 84, 102, 114]. Note that in the case of snoring these assumptions would certainly be discutable.
Thirdly the Reynolds number, $Re = \frac{\rho_0 U_0 h_0}{\mu_0}$ with U_0 a typical flow velocity, h_0 a typical dimension (such as the pharyngeal minimum aperture), μ_0 the dynamic viscosity and ρ_0 the density, represents the importance of inertial forces with respect to the viscous forces acting on a given fluid element and the length of the pharyngeal replica. In first approximation the flow is assumed to be inviscid considering the involved characteristic Reynolds numbers $Re_0 \approx O(10^3)$. Although it can be neglected for the bulk of the flow, viscosity is important near the walls motivating the application of the boundary layer theory. Next, the occurrence of flow separation is a consequence of the viscosity and has a strong influence on flow control [76, 84]. Therefore the flow separation point is either considered to be fixed by an empirical 'ad-hoc' assumption or is predicted based on physical principles. The relevance of this assumption and its influence on the position of flow separation is extensively investigated in this paper.
Fourthly, the ratio of characteristic geometrical lengths yields information about the dimensionality of the flow. The aspect ratio h_0/W_0 is considered, with h_0 a typical minimum aperture and W_0 a typical width. Following the characteristic ratio $h_0/W_0 = 0.09$ [$h_0/W_0 << 1$] the flow is assumed to be characterised by a bidimensional flow description in the (x,y)-plane. This assumption will be experimentally tested.
In the next subsection different flow descriptions are presented based on the assumptions with respect to viscosity, dimensionality of the flow description and to the influence of the

asymmetry on the geometrical replica. As a result the flow predictions resulting from different simplifications of the bidimensional laminar, incompressible and quasi-steady Navier Stokes (NS) equations can be numerically and experimentally validated.

7.2 Theoretical flow predictions

The origin of OSA lies in a strong interaction of the fluid and the surrounding tissue provoking the pharyngeal airway recurrently to collapse during sleep. A first requirement to describe ongoing phenomena is to know the pressure variations through the pharyngeal geometry. Since an exact analytical solution for the flow through such a constriction is not available different flow models and flow assumptions are assessed to estimate 1) the volume flow velocity ϕ and 2) the pressure distribution p(x) as function of position [12, 96].
Once p(x) is known the force F(x) acting by the airflow on the surrounding tissue of the pharynx is deduced as $F(x) = \int pdS$.

7.2.1 Bernoulli with ad-hoc viscosity correction

In first approximation, the flow is assumed to be fully inviscid. The three assumptions of incompressible, quasi-steady and inviscid flow allow to apply the steady one-dimensional (1D) Bernoulli law (1),

$$p(x) + \frac{1}{2}\rho U(x)^2 = cte, \tag{1}$$

to estimate the pressure distribution p(x) along the pharyngeal walls. The volume flow velocity is defined by $\phi(x) = U(x)A(x) = cte$ with $U(x)$ the local flow velocity and $A(x)$ the area along the pharyngeal replica. To be useful, an empirical ad-hoc correction is needed to the 1-D Bernoulli equation to account for the occurrence of flow separation downstream of h_c. The jet formation downstream of the point of flow separation is due to very strong viscous pressure losses and reversed flow occurring near the wall and thus can not be predicted by the Bernoulli law. For a steady flow the onset of separation coinciding with the separation point is defined as $\frac{\partial U}{\partial n}|_{n=0} = 0$. In literature, the area associated with flow separation A_s is empirically chosen as 1.2 times the minimum area A_{min} along the replica, i.e. $A_s = cA_{min}$, with $c = \frac{A_s}{A_{min}} = 1.2$ [45, 83]. The ad-hoc correction for the 1D Bernoulli (1) results in a steady 1D expression for $p(x)$ given in (2), with p_0 and A_0 respectively the upstream pressure and area. The volume flow velocity is estimated as (3). In expression of (2) pressure recovery downstream of the point of flow separation is neglected.

$$p(x) = p_0 + \frac{1}{2}\rho\phi^2\left(\frac{1}{A_0^2} - \frac{1}{A(x)^2}\right) \tag{2}$$

$$\phi = A_s\sqrt{\frac{2(p_0)}{\rho}}, A_s = cA_{min} \tag{3}$$

The preceding assumption of inviscid flow is not valid for low Reynolds numbers. This is the case for low flow velocities U or/and small h_c values. In this case, an extra Poiseuille term is often added to the Bernoulli expression for p(x) in (2) to correct for viscous pressure losses. The Bernoulli expression with Poiseuille correction is given in (4) with μ the dynamic viscosity coefficient, W the width of the half cylinder and h(x) the height between the half cylinder and the flat plate as defined in subsection 7.3.1 and depicted in Figure 1.

$$p(x) = p_0 + \frac{1}{2}\rho\phi^2\left(\frac{1}{A_0^2} - \frac{1}{A(x)^2}\right) - \frac{12\mu\phi}{W}\int\frac{dx}{h(x)^3} \tag{4}$$

7.2.2 Boundary layer solution

In the preceding subsection 7.2.1 the viscosity is either neglected (Bernoulli in (2)) or corrected with an additional Poiseuille term, assuming a fully developed Poiseuille flow (Poiseuille in (4)). However, at high Reynolds numbers the region in which viscous forces are important is confined to a thin layer adjacent to the wall which is referred to as laminar boundary layer δ. Outside of the boundary layer, the inviscid irrotational main flow, with velocity U(x), is described by Bernoulli (3). The resulting boundary layer theory is described by the Von Kármán momentum integral equation for steady flows [96]. An approximated method to solve this equation for laminar incompressible bidimensional (x,y) boundary layers is given by Thwaites method.
Introducing two shape parameters $H(\lambda) = \frac{\delta_1}{\delta_2}$, $S(\lambda) \propto \frac{\tau_S\delta_2}{U}$ which are only functions of the velocity profile determined by the acceleration parameter $\lambda \propto \frac{dU}{dx}\delta_2$, with $\tau_S(x) \propto \lim_{n\to 0}\frac{\partial u}{\partial n}$ the wall shear stress indicating the viscous force per unit area acting at the wall, the displacement thickness δ_1

$$\delta_1(x) = \int_0^\infty \left(1 - \frac{u(y)}{U}\right)dy, \tag{5}$$

and the momentum thickness δ_2

$$\delta_2(x) = \int_0^\infty \frac{u(y)}{U}\left(1 - \frac{u(y)}{U}\right)dy. \tag{6}$$

The Von Kármán equation is then approximated by

$$\delta_2^2(x)U^6(x) - \delta_2^2(0)U^6(0) \propto \int_0^x U^5(x)dx. \tag{7}$$

Equation (7) in combination with the fitted formulae for H(λ) and S(λ) tabulated in [12] enables to compute the strived pressure distribution $p(x)$ up to the flow separation point where $\tau_S = 0$ for a given input pressure and known geometry. Moreover, the point

of flow separation x_S is numerically estimated since separation is predicted to occur at $\lambda(x_S) = -0.0992$ [85]. So no ad-hoc assumption is made to account for flow separation. In [28] the method was successfully applied to accurately predict the position of flow separation and associated pressure within the glottis. In the present study the prediction of the pressure distribution along the pharyngeal replica is assessed. Although since flow prediction downstream of the position of flow separation is not possible in the following subsections a numerical methods of flow prediction is outlined.

7.2.3 Reduced Navier Stokes

A second simplification of the Newtonian steady laminar incompressible bidimensional Navier Stokes equations is obtained making two additional assumptions. Firstly the flow is assumed to be characterised by a large Reynolds number and secondly the geometrical transverse dimension (y-axis) is assumed to be small compared to the longitudinal dimension (x-axis). In the geometry under study the last assumption coincides with $h_0 << D$. Applying those assumptions to the bidimensional NS equations results in a system in which the transverse pressure variations are neglected. This system is referred to as the Reduced Navier Stokes/Prandtl (RNSP) system in accordance with Prandtl's formulation of the steady boundary-layer [58]. Nondimensional variables are obtained by scaling u^* with U_0, v^* with U_0/Re, x^* with $h_0 Re$, y^* with h_0 and p^* with ρU_0^2 with the Reynolds number defined as $Re = U_0 h_0/\nu$. In terms of the nondimensional variables the resulting RNSP equations become:

$$\frac{\partial}{\partial x}u + \frac{\partial}{\partial y}v = 0, \qquad u\frac{\partial}{\partial x}u + v\frac{\partial}{\partial y}u = -\frac{\partial}{\partial x}p + \frac{\partial^2}{\partial y^2}u, \qquad 0 = -\frac{\partial}{\partial y}p. \tag{8}$$

The no slip boundary condition is applied to the lower and upper wall. Since the lower wall of the geometry of interest corresponds to $y = 0$ and the distance to the upper wall is denoted with $h(x)$ the no slip condition becomes respectively ($u(x, y = 0) = 0$, $v(x, y = 0) = 0$) and ($u(x, y = h(x)) = 0$, $v(x, y = h(x)) = 0$). In order to numerically solve the RNSP equations the pressure at the entrance is set to zero and the first velocity profile need to be known (Poiseuille). There is no output condition.

7.3 Experimental validation

In order to enable experimental validation of the predicted pressure distribution for a given pressure, a suitable 'in-vitro' pharyngeal replica and experimental setup is required. Next, the flow predictions outlined in section 7.2 are developed assuming particular flow conditions. Therefore major flow assumptions discussed and motivated in subsection 7.1 are experimentally validated before in the following section the predictive value of the flow descriptions is systematically explored.

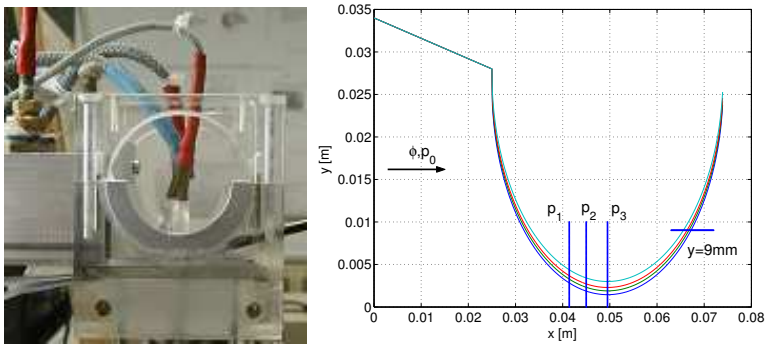

(a) photograph (b) schematic overview

Figure 1: (a) Photograph of the 'in-vitro' pharyngeal tongue replica, mounted pressure transducers and hot film. (b) Schematic 2D overview of the 'in-vitro' pharyngeal tongue replica, mounted pressure transducers and hot film. The pharyngeal cavity geometry is represented by a flat bottom plate corresponding to y=0 and half cylinders with diameter D=49 mm for the assessed h_c's (1.45, 1.90, 2.30 and 3.00 mm). The y-axis corresponds with the distance between the flat plate and the half cylinder. The x-axis presents the distance along the longitudinal axis of the replica. The sensor sites are indicated with a solid blue line. The direction of incoming airflow is indicated with an arrow.

7.3.1 In-vitro pharyngeal rigid tongue replica

The place of obstruction in the pharynx at the origin of OSA is known to be very variable (naso-, oro- or laryngopharynx) [91]. Regardless the precise location of obstruction in the pharynx the relevant anatomy is 'in-vitro' imitated by a rigid half cylinder, representing roughly the tongue geometry, placed inside a rectangular uniform pipe representing thus the pharyngeal wall. Changing the minimum aperture (h_c) between the tongue-replica and the pipe allows the study of different obstruction configurations. Consequently the important geometrical parameters are the diameter D of the half cylinder and the value of h_c. In this study the diameter D of the rigid replica is fixed to 49 mm which is in accordance with anatomical 'in-vivo' values. Different degrees of constriction are studied by changing h_c between the half cylinder and the flat plate. Minimum distances h_c of 1.45, 1.90, 2.30 and 3.00 mm are considered. These distances were measured using calibrated plates with an accuracy of 0.01 mm. In order to connect the replica to the experimental setup described in subsection 7.3.2 a triangular attachment of length 25 mm and height 6 mm is fasten to the upper part of the half cylinder maintaining a fixed vertical height of h_0=34 mm between the beginning of the attachment and the flat plate. A photograph and longitudinal cross-section of the resulting pharyngeal geometry constituted from the attachment and 'in-vitro' tongue replica is depicted in respectively Figure 1(a) and Figure 1(b) for the assessed h_c's. The flat plate coincides with the x-axis at y=0. The changing height of the replica along the x-axis is further denoted with $h(x)$. Remark the physiologically observed strong asymmetrical nature of the replicas geometry in the (x,y)-plane. The replica has a fixed width W of 34

mm along the z-dimension.

7.3.2 Experimental setup

To simulate the origin of OSA the rigid pharyngeal replica is attached to an 'in-vitro' test-installation. The test-installation enables to study the influence of various upstream pharyngeal airflow conditions. To validate theoretical flow predictions, flow characteristics are measured at different positions along and upstream of the tongue replica. Incoming airflow conditions are determined by measuring the volume flow velocity (ϕ) and upstream pressure (p_0) as indicated in Figure 1(b). The volume flow velocity ϕ [l/min] is measured using a thermal mass flow meter (TSI 4040) with an accuracy of 0.01 l/min. Flow pressure measurements [Pa] are performed at three different positions (p_1, p_2, p_3) depicted in Figure 1(b) along the converging part of the rigid tongue replica and the flat bottom plate. The pressure is measured with piezoresistive pressure transducers (Endevco 8507C or Kulite XCS-093) positioned in pressure taps of 0.4 mm diameter at the mentioned sites which allows dynamic pressure measurements. The site p_3 corresponds to the position h_c. The sites p_2 and p_1 are respectively located upstream from the site p_3 at 4.5 mm and 8.0 mm along the x-dimension. The pressure transducers are calibrated against a water manometer with an accuracy of 1 Pa. The volume flow velocity ϕ and pressure distribution p(x) along the replica are predicted from the measured upstream pressure p_0.
Next to pressure measurements a constant temperature anemometer system (IFA 300) is available in the test-installation to perform flow velocity measurements with accuracy of 0.1 m.s^{-1}. Velocity profiles can be obtained by moving the hot film using a two dimensional stage positioning system (Chuo precision industrial co. CAT-C, ALS-250-C2P and ALS-115-E1P). The accuracy of positioning in the x and y direction is respectively 4 and 2 μm.

7.3.3 Experimental validation of some major flow assumptions

Spatial distribution of the flow

The steady flow models presented in section 7.2 result in a 1D, quasi-2D or 2D flow description. The third dimension (z-axis) perpendicular to the (x,y) plane is assumed to have no influence on the flow. In order to validate this assumption, the horizontal velocity profile is measured for each h_c. Figure 2(a) illustrates an exemplary velocity profile for $h_c = 2.3$ mm and a steady flow of 60 l/min. The step Δz at the edges near the wall is 0.1 mm elsewhere Δz equals 1.0 mm. The anemometer is positioned as close as possible to the minimum aperture. The measured velocity has a standard deviation (ξ [%]) $\xi < 1$ % around its mean value. $\xi < 1$ % corresponds to a flat velocity profile along the z-direction. For all assessed apertures and volume flow rates $\xi < 1$ % is maintained. At

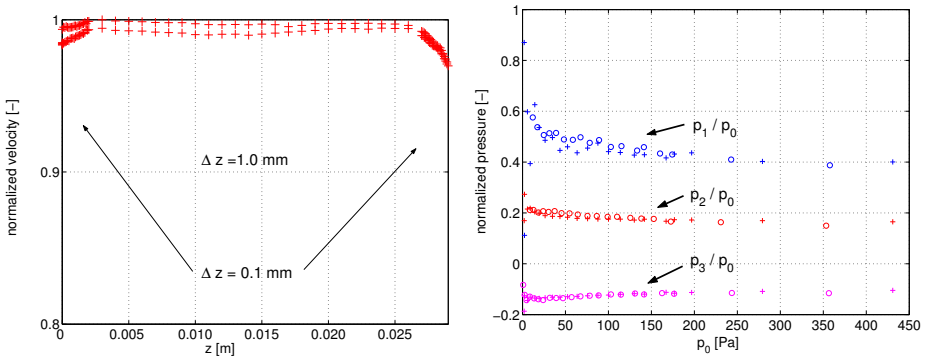

(a) horizontal velocity profile (b) pressure measurements

Figure 2: (a) Normalized horizontal velocity profile (0 up to 30 mm and 30 down to 0 mm) for $h_c = 2.3$ mm and a steady flow of 60 l/min. (b) Pressure measurements at p_1, p_2 and p_3 normalized with the upstream pressure p_0 for $h_c = 3.00$ mm. Pressures are measured on the half cylinder (+) and on the flat bottom plate (o).

the edges, where a smaller step size of Δz = 0.1 mm is applied, the measured velocities are slightly decreased due to the presence of the boundary layer. Consequently neglecting the z-dimension in the flow description is positively validated and as such a bidimensional (x,y) spacial distribution of the flow is motivated.

The velocity profiles depicted following the y-dimension in figure 3(b) draw attention to the asymmetry of the flow within the pharyngeal replica. The vertical velocity along the y-dimension is measured while the x-value coincides with an aperture of 9 mm along the diverging side of the replica. This position is indicated by the horizontal line at h(x)=y=9 mm in Figure 1(b). The vertical velocity profile is measured with a spatial resolution of Δz = 0.1 mm. Figure 3(b) shows the vertical velocity profile for volume flow velocities ranging from 20 l/min up to 100 l/min for a minimum aperture $h_c = 2.30$ mm. y=0 corresponds with the flat plate of the replica. For high volume flow velocities the vertical velocity profiles in figure 3(b) becomes asymmetrical. In order to evaluate the impact of the asymmetry on the pressure distribution the pressure is measured at positions p_1, p_2 and p_3 on the half cylinder as well as on the flat bottom plate as indicated in figure 1(b). Figure 2 represents an example of the normalized pressure measurements for different values of the upstream pressure p_0 for the minimum aperture $h_c = 3.00$ mm. At the position of the minimum aperture the ratio $\frac{p_3}{p_0}$ approximates -0.15 for both the pressures measured on the half cylinder as on the flat bottom plate. This ratio is of the same order of magnitude than the one mentioned in [45] for a symmetrical lip replica with a comparable minimum aperture of $h_c = 3.36$ mm. Thus at the position of minimum aperture the measured pressure difference is between the half cylinder and the flat plate is very limited. The pressures measured at the flat plate at position p_2 are by a few percent superior to the pressures measured at the half cylinder. Looking at the measurements at position p_1 the

same finding holds. Furthermore the transverse pressure difference is found to decrease approaching the minimum aperture. So the influence of the asymmetry on the pressure measurements augments with increasing absolute value of the spatial derivative. Although systematically, the measured pressure gradients at positions p_2 and p_1 are far inferior to 10 %, which is small compared to the general accepted error range of 25 % [45]. Same findings hold for all assessed minimum apertures. Therefore it is concluded that although measurable, the asymmetry hardly affects transverse pressure measurements and thus the strived pressure distribution p(x). This finding is important considering application of the boundary layer theory since, as expressed in equation 8, the equations of motion within the boundary layer assume that transverse pressure variations can be neglected. The experimental findings are in agreement with theoretical modelling results presented in [59]. Firstly the measured tendency is confirmed, i.e. increasing the pressure drop on the curved wall and decreasing is on the other. Secondly, the effect is found to be second order, so the effect is small but measurable. The theoretical results are obtained with both a Navier-Stokes solution as with an integral interacting boundary layer (IBL) theory for steady laminar flow in a asymmetrical bidimensional channel at high Reynolds number. Although the IBL method is very fast at present the second order effect is further left out of consideration, but might be applied in future since the asymmetry also influences the position of minimum pressure and flow separation [59].

Flow prediction

Figure 3(a) illustrates a detailed bidimensional velocity map for a steady flow of 40 l/min with a minimum aperture of h_c = 3.00 mm. The presented findings hold for all assessed minimum apertures and volume flow velocities. The anemometer is displaced with a step of Δx = 1 mm in the x direction and Δy = 0.05 mm in the y direction. The same way as for the horizontal velocity profile depicted in Figure 2(a) the decrease in velocity towards the edges provides experimental evidence for the presence of a boundary layer. Along the diverging part of the replica the velocity tends to zero, which experimentally illustrates the impact of flow separation on the flow also mentioned in [102]. The importance of the boundary layer and flow separation on the bidimensional flow description is further illustrated in figure 3(b). The plotted profiles show the existence of a boundary layer near the edge (y/$h_c = 0$) and the formation of a jet since the velocity tends to 0 as the ratio y/h_c becomes superior to 1. The development of the inviscid main flow with increasing volume flow velocity is clearly illustrated. Due to the importance of the position of flow separation on the flow control in the following the relevance of the assumption with respect to a fixed or predicted flow separation point are extensively considered with respect to the strived pressure distribution.

The ad-hoc corrected Bernoulli law with the assumption of fixed flow separation point described in subsection 7.2.1 results in the crudest prediction of the strived pressure distribution. The application of the one dimensional pressure prediction is illustrated in figure 4(a)

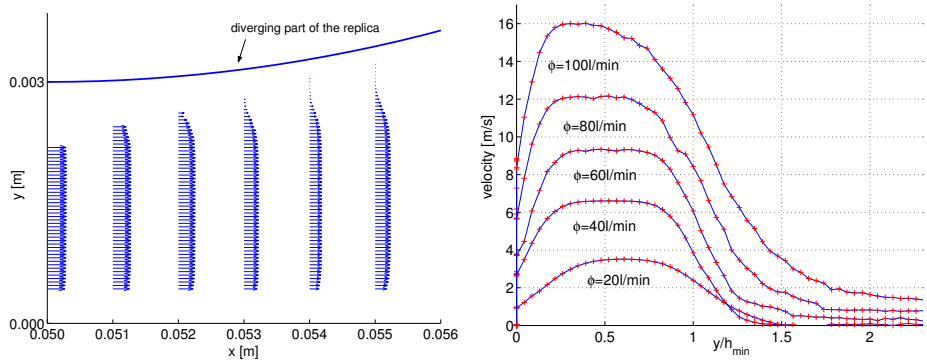

(a) bidimensional (b) vertical

Figure 3: (a) Measured bidimensional velocity profile (absolute value) illustrating flow separation and jet formation along the diverging part of the replica for a steady flow of 40 l/min and $h_c = 3.00$ mm. A step of $\Delta x = 1$ mm in the x direction and $\Delta y = 0.05$ mm in the y direction is applied. (b) Measured vertical (along the y-axis) velocity profile at y=9 mm for given flow velocities ϕ with $h_c = 2.30$ mm. Note the asymmetrical behaviour for ϕ=100 l/min.

for a minimum aperture $h_c = 1.45$ mm. The volume flow velocity ϕ is varied from 5 up to 120 l/min in steps of 5 l/min (Re $\leq$ 4719). The ratio of the measured and upstream pressure p_0 at the positions p_1, p_2 and p_3 are indicated with crosses. The one dimensional pressure distribution p(x) is shown for two different positions of flow separation expressed by two values of the constant $c = \frac{A_s}{A_{min}}$. The constant c is chosen to 1.2 and 1.05 corresponding to respectively the value proposed in literature and the value retrieved from the measured data $c = \sqrt{1 - \frac{p_3}{p_0}} = 1.05$. Remark that in the last case the modelling performance is optimized by using not only one input value (p_0), but two (p_0,p_3). Since p_3 is used as an input the predicted pressure values at position p_3 are expected to correspond well with the measured pressures. The origin of the OSA syndrome is qualitatively explained by the negative pressure at the level of the constriction. As expected an accurate quantitative model is obtained for the region of maximal pressure drop (R^2=0.99 at site p_3) from the 1D flow description. The impact of the 'ad-hoc' value c or the position of flow separation on the predicted pressure distribution is obvious. Consequently the position of flow separation (or the value of the constant c) will largely affect the forces exerted by the flow on the surrounding tissues. In order to further evaluate the retrieved constant $c = 1.05$ figure 5 shows the physical value of the constant c predicted using Thwaites method and RNSP. It appears that the ad-hoc value c=1.05 greatly underestimates the position of flow separation x_S for all covered volume flow velocities. So, although the ad-hoc value c=1.05 optimises the 1D modeling performance, it is an unphysical value resulting in a less accurate force distribution. As the matter of fact, since:

$$F = W \int_{inlet}^{separation} p(x)dx, \tag{9}$$

so accurate prediction of separation point absence is also of importance and one dimensional

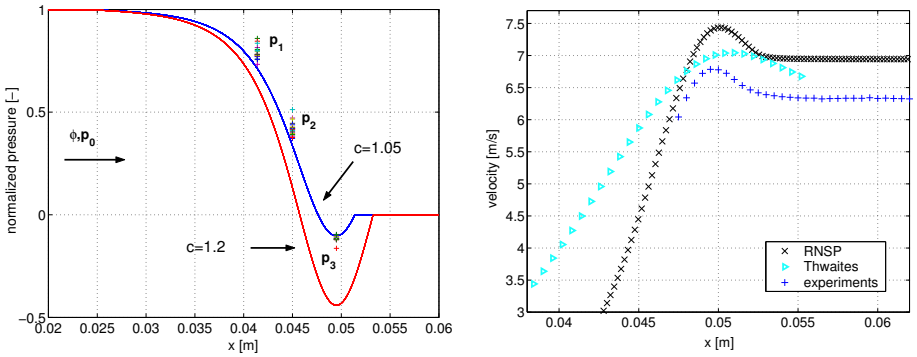

(a) pressure (b) velocity profile

Figure 4: (a) Pressure measurements along the half cylinder at p_1, p_2 and p_3 (+) and Bernoulli simulations with c=1.05 (full line on top) and c=1.2 (full line below) normalised with the upstream pressure p_0 for $h_c = 1.45$ mm and ϕ=5 l/min up to ϕ=120 l/min. (b) Longitudinal velocity profile with a step of $\Delta x = 1.0$ mm for $h_c = 3.00$ mm and ϕ=40 l/min: measured data (+), Thwaites (▷) and RNSP (x).

pressure prediction involving a fixed position of the flow separation point is not useful for application to OSA where the force distribution is important and will not be considered further. This finding is in agreement with [76, 84] who stresses the importance of an accurate prediction of flow separation and the need to improve the one-dimensional model with more modern boundary layer methods.

Figure 4(b) shows the measured and predicted longitudinal velocity profile along the x-axis using Thwaites method and RNSP, outlined in subsections 7.2.2 and 7.2.3 for a steady flow of 40 l/min with a minimum aperture $h_c = 3.00$ mm. Note the limited range of experimental data along the longitudinal dimension, i.e. the x-axis. This is due to the physical dimensions of the hot film probe preventing further insertion inside the replica. Thwaites method does not allow to compute any predictions past the point of flow separation. Consequently for large x values only experimental data points and RNSP predictions can be seen. The same findings hold for all assessed minimum apertures and volume flow velocities.

The velocity values obtained with both Thwaites method and RNSP are within 10 % agreement with the measured velocity values. Although the velocity distribution within the replica seems much more accurate with RNSP since the trend in the measured data is captured.

7.3.4 Pressure distribution

The predictive value of the bidimensional flow predictions using Thwaites method and RNSP is quantitatively explored in [110]. Since the position of flow separation largely affects the force distribution, we reconsider the predicted values of the constant c for different volume flow velocities depicted in figure 5. Although very close, the constant predicted

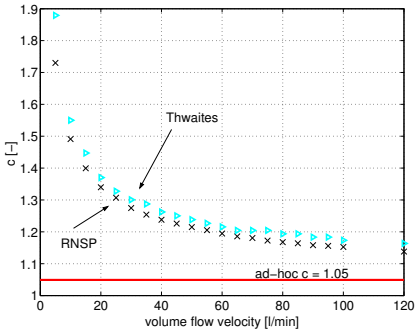

Figure 5: c [-] as function of ϕ predicted from Thwaites (▷), RNSP (x) and the ad hoc constant c=1.05 (full line) for $h_c = 1.45$ mm.

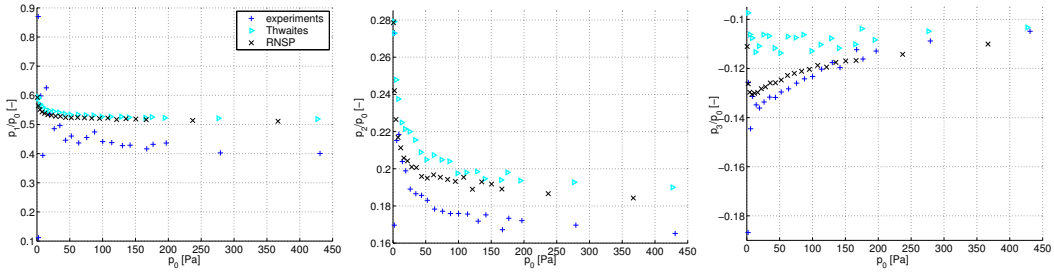

(a) (b) (c)

Figure 6: Normalized pressure for $h_c = 3.00$ mm at position (a) p_1, (b) p_2 and (c) p_3: measured data (+), Thwaites (▷) and RNSP (x).

with Thwaites is systematically superior to the constant obtained from RNSP. Consequently RNSP predicts flow separation to occur prior compared to Thwaites. To evaluate the prediction of the pressure distribution with Thwaites and RNSP the pressures measured at positions p_1, p_2 and p_3 are compared to the computed pressures. Figures 6(a), 6(b) and 6(c) show the predicted and measured data normalised by the upstream pressure p_0 at positions p_1, p_2 and p_3 for $h_c = 3.0$ mm as function of the upstream pressure p_0. In general the pressure drop predicted by RNSP is slightly superior to the pressure drop predicted by Thwaites method. A larger pressure drop agrees with the slightly inferior value of the constant c mentioned earlier in case of RNSP. Figure 6(c) illustrate that both Thwaites and RNSP pressure predictions at the minimum aperture p_3 yields well within the typically accepted error range of 25 % on the measured pressure values [45]. From the remaining figures it can be seen that this hold also for the pressure measured at positions p_1 and p_2. Note from Figure 4(a) that using Bernoulli would give estimation errors far above the accepted error range of 25 % in case the position of flow separation is respected (c=1.2). The overall model performance for all assessed minimum apertures (1.45, 1.90, 2.30, 3.00 mm) at the positions p_1, p_2 and p_3 for Thwaites and RNSP is detailed in [110] for volume flow velocities ranging from 5 l/min to respectively $\leq$30, $\leq$60, $\leq$80, $\leq$100 and $\leq$120 l/min. The covered ranges

allow to value the predictive value for distinct Reynolds numbers $Re = \frac{\phi}{W\nu}$, with ν being the kinematic viscosity coefficient and W and ϕ as defined previously. For all 5 cases the model performance of both Thwaites and RNSP at the position of minimum constriction is excellent. Further it can be seen that in the prediction performance increases approaching the position of minimum aperture. This finding stresses the importance to validate the pressure predictions at different sites along the replica in order to compare and evaluate flow predictions if the pressure distribution and hence the forces exerted by the flow on the surrounding walls is of interest. Reynolds numbers below 2500 are characteristic for laminar flows. Higher values of the Reynolds number indicate the transition from laminar to turbulent or turbulent flows. Since the applied bidimensional flow predictions are laminar flow models the flow behaviour was expected to be most accurately described within the laminar range, as is the case. Furthermore the predictive value of RNSP exceeds slightly Thwaites predictions for low volume flow velocities in the laminar range. The volume flow velocities involved during OSA are below 30 l/min [32]. So, in case of OSA the predictive value of RNSP exceeds slightly the predictive value of Thwaites method and RNSP prediction is favoured to acquire the pressure distribution.
The obtained results experimentally confirms the numerical study reported in [102] for a rigid pharyngeal geometry and in particular the crucial effects of geometrical changes in the morphology. The minimum aperture or the degree of obstruction on the pressure drop is systematically varied in order to explore the influence of small geometrical changes as e.g. caused by surgery. In addition, the applied 'in-vitro' methodology allows validation of major theoretical hypothesis and quantification of the flow model performance. Since measuring flow characteristics and hence theoretical model validation inside an oscillating elastic tube is a difficult task, the presented experimental validation is a necessary step towards flow modeling in case of a non-rigid collapsible replica as presented in the next section.

8 Towards an accurate simplified fluid structure model

Experimental validation under controlled and measurable experimental conditions on a non-rigid elastic replica is the next crucial step before extending the findings to a true human pharynx and preliminary prediction of surgical interventions.

8.1 In-vitro pharyngeal deformable tongue replica

As an alternative to the classical Starling resistor a deformable 'in-vitro' pharyngeal tongue replica is presented. The design is inspired on a mix of the rigid 'in-vitro' pharyngeal tongue replica described in 7.3.1 and 'in-vitro' deformable replicas of the vocal folds [24, 94, 95, 109]. The same way as for the rigid replica the relevant 'in-vivo' anatomy is simplified and 'in-vitro' imitated by a metal cylinder representing roughly the tongue geometry covered

with latex of 0.3 mm thickness. Different stages of mounting are illustrated in Figure 7. The covered cylinder is placed inside a rigid circular uniform pipe of diameter 25 mm.

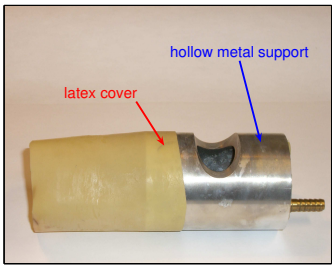

(a) cover and support

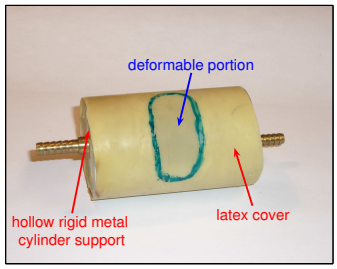

(b) upper cylinder

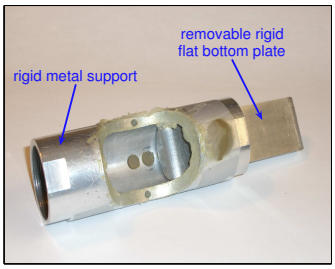

(c) support and flat pate

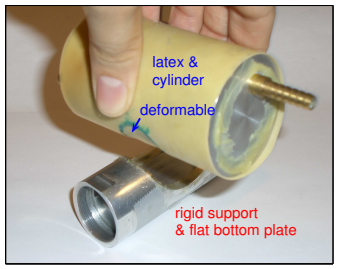

(d) mounting

Figure 7: Mounting of the deformable tongue replica. (a) Latex cover and rigid support, (b) Resulting deformable upper cylinder, (c) rigid support and removable flat bottom plate and (d) Mounting the deformable 'in-vitro' tongue replica.

The metal cylinder has the same diameter of 49 mm as the rigid replica. The interior is hollow so the covered cylinder can be filled with water supplied through small ducts of 4mm diameter connected to a water column. The height of the water column is controllable. This way the internal pressure P_{in} is controllable as well. A portion of the metal cylinder is removed, with internal length 27 and width 22 mm, in order to obtain a deformable part which fit in the metal circular pipe support. Mounting of the cylinder to the rigid pipe support provides a constricted channel for the airflow. A removable rigid flat bottom plate is inserted representing thus the pharyngeal wall. The choice of the flat plate influences the height of the constriction between the cylinder and the bottom plate. The centre height of the constriction h_c corresponds to the requested geometrical input parameter for theoretical modelling and is indicated in Figure 8(a) illustrating the mounted replica. Besides the bottom plate the initial degree of obstruction, i.e. in absence of airflow, in the channel formed between the cylinder and the flat plate is altered by imposing the internal pressure P_{in} lifting or lowering the water column connected to the water supply. Initial obstruction heights h_c of maximal 3 mm are assessed corresponding to obstruction degrees of more than

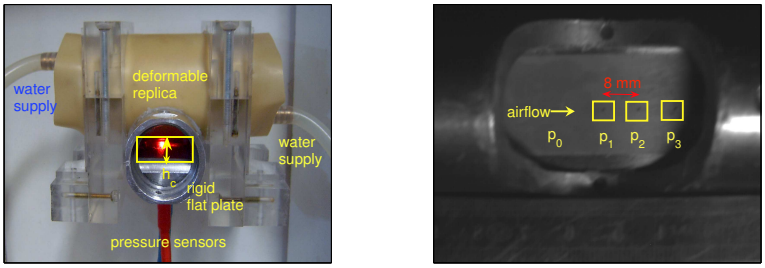

(a) frontal view at downstream end (b) upper view support

Figure 8: (a) Frontal view of the mounted deformable replica at downstream end. The deformable area is indicated with a rectangle. The laser spot allows to make dynamical measurements of the centre height h_c. Pressure sensors are mounted on the rigid flat bottom plate at positions inidicated in part b. The water supply allows to control the internal pressure in the replica. (b) Longitudinal upper view of the mounted rigid flat bottom plate in absence of the latex cylinder with pressure taps.

90 % reckoning for the upstream pipe diameter of 25 mm. The imposed P_{in} determines also the mechanical properties of the deformable replica. Pressure taps of 0.4 mm diameter are positioned upstream of the replica and along the diverging part of the constriction in the removable bottom plate at a distance of 8 mm. The exact position is indicated in Figure 8(b) with a square for the pressure taps p_1, p_2 and p_3 and p_0 denotes the upstream pressure. Note that the position p_1 coincides with the centre of the metal support cylinder, so with the rigid minimum constriction of the undeformed cylinder.

8.2 Experimental setup and collapse model

An air supply is connected to a pressure tank of 0.75 m^3 enabling to impose an airflow through the flow channel of the deformable replica. The same way as for the rigid replica pressure sensors (Endevco 8507C or Kulite XCS-093) are positioned in the pressure taps enabling to quantify the pressure distribution at positions (p_0, p_1, p_2, p_3) where p_0 determines the pressure difference ΔP between upstream and downstream pressure of the constriction which is the main driving parameter of the studied fluid-structure interaction. The geometry and the deformation of the replica can be observed by means of a laser beam (635 nm) passing through the replica and brought to focus on a light sensitive diode (BPW 34) [109]. As can be observed in Figure 8(a), the width of the laser beam covers only a limited part of the width of the open area A between the bottom plate and the deformable upper part indicated by the rectangle on Figure 8(a). Therefore the optical laser system was calibrated to relate the transmitted light intensity of the original beam to the centre height (h_c) between the bottom plate and the curved upper part. This way time-varying centre heights $h_c(t)$ up to 6 mm can be measured with an accuracy of 0.01 mm. Besides the optical laser system a camera-based visualization system detailed in [109] is applied to monitor the deformation

of the geometry. Imaging with a digital camera (Inca311 with resolution 1280x1024 pixels, Philips) is triggered with respect to the upstream pressure p_0 in order to acquire images of the open area A at different stages during the fluid-structure interaction, enabling visualization of different degrees of deformation and hence variations of the original open area A^0. More particularly, a step-trigger is acquired whenever p_0 is gradually increased (between 0 and $\pm$2500 Pa) and an image is acquired whenever p_0 is raised with a fixed step of 50 Pa. Consecutive images are shown in Figure 9. A collapse of the deformable replica due to the interaction with the airflow is observed. Consequently the proposed replica is capable to

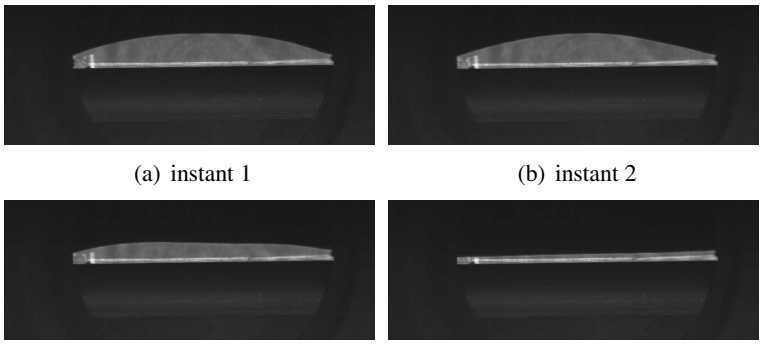

(a) instant 1 (b) instant 2

(c) instant 3 (d) instant 4

Figure 9: Visualisation of 'in-vitro' replica deformation at consecutive time instants. The visualised area is indicated with a rectangle in Figure 8(a). So the bottom of the images corresponds to the rigid flat bottom plate and the top with the deformable part of the latex cylinder.

reproduce 'in-vitro' a partial collapse characteristic for a hypopnea. The reproduction of a total collapse, corresponding to an apnea, is illustrated in Figure 10 by way of a simple dye experiment. The deformable part is coloured. Observation of the dye deposit on the flat

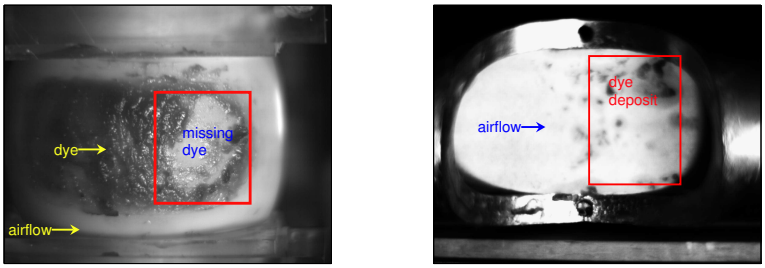

(a) dye suppress on latex cylinder (b) dye deposit on rigid flat plate

Figure 10: Deposit from dye of the deformable upper part (a) on the rigid flat plate (b) after a fluid-structure interaction illustrating contact or a total collapse of the deformable tongue replica shown in 8 as well as an important movement in the flow direction.

bottom plate when p_0 is increased allows firstly to put in to evidence complete closure of

the replica and secondly a movement of the deformable part in the airflow direction during closure.
Both the camera observations and the simple dye experiment, shown in Figures 9 and 10 respectively, illustrate that the proposed replica is suitable to reproduce partial or complete collapse. The proposed replica is therefore an alternative to the classical Starling resistor experiment. Furthermore despite the severe simplifications the current replica design allows to study the influence of asymmetrical wall characteristics, to measure and hence to validate the pressure distribution along the flat bottom plate and to quantify the deformation for several constriction heights depending on the bottom plate and the imposed internal water pressure P_{in} in the cylinder.

8.3 Simplified fluid structure interaction model

The fluid structure interaction between a fluid flow model and a mechanical structure model is schematically depicted in Figure 11. An iterative procedure [43] enables to model the

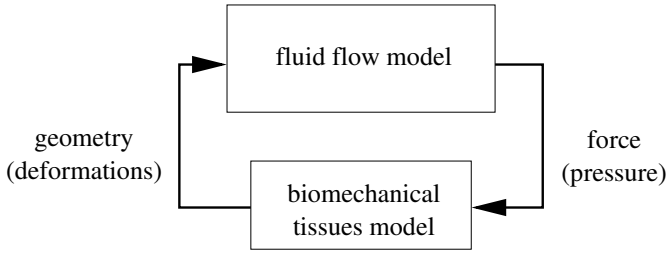

Figure 11: Schematic representation of segregated physical modelling of flow-structure interactions.

fluid structure interaction on the deformable replica described in 8.1 and illustrated in the previous section 8.2. First the pressure distribution is computed using the RNSP flow model which is detailed and motivated in section 7. Next the corresponding forces are applied to a finite element model of the 'in-vitro' setup presented in [16, 18] resulting in a deformation of the initial geometry. Then the flow model is again applied to compute the pressure distribution resulting in a new deformation. This procedure is iterated until the yielded deformation is no more significant. The whole procedure is detailed in [16, 18]. Very briefly a finite element three-dimensional model of the deformable part of the replica is proposed accounting for its geometry, mechanical characteristics and boundary conditions. As the fluid model is assumed to be two-dimensional and the structural model is three-dimensional, the structure is divided into a small number of 5 slices and the pressure distribution is computed for each element. The Poissons ratio is set to $\mu = 0.499$ assuming incompressibility. The Young modulus E is fixed to 1.6 MPa in agreement with 'in-vitro' experimental deformation h_c data obtained in absence of airflow for different internal pressures P_{in} and assuming small deformations and a linear relationship between constraint and deformation [16, 18].

Figure 12 illustrates typical examples of the constriction height $h_c(t)$ for ΔP increased to 200 and 290 Pa, the initial centre heights h_c^0 yield 1.2 and 0.87 mm, respectively, and P_{in} is fixed to 200 and 400 Pa. The centre height h_c is obtained by means of a laser beam as

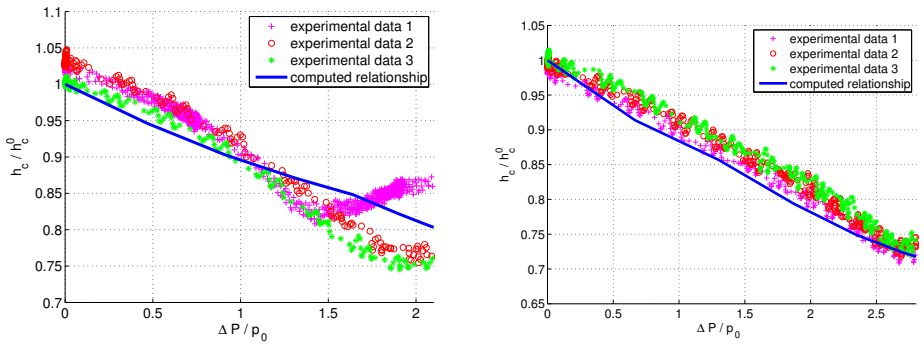

(a) ΔP=200Pa, h_c^0=1.2mm, P_{in}=200Pa (b) ΔP=290Pa, h_c^0=0.87mm, P_{in}=400Pa

Figure 12: Simulation of a hypopnea illustrating measured (+,○,∗) and predicted (full line) centre height h_c as a function of upstream pressure [16, 18].

explained in section 8.2. Since the imposed P_{in} value in 12(b) is greater than the value imposed in 12(a) the initial aperture in 12(b) is smaller than in 12(b). The reproducibility of the data is thoroughly validated by performing multiple experiments as shown in Figure 12. The experimental results correspond to a collapse of about 25 % corresponding to the 'in-vitro' reproduction of a hypopnea syndrome due to the negative pressure forces along the constriction as extensively discussed in section 7.3 for the rigid replica. The occurrence of negative pressures measured on the deformable replica is illustrated in Figure 13 for P_{in} set to 200 Pa. The pressure is measured at the pressure taps p_1, p_2 and p_3 shown in Fig-

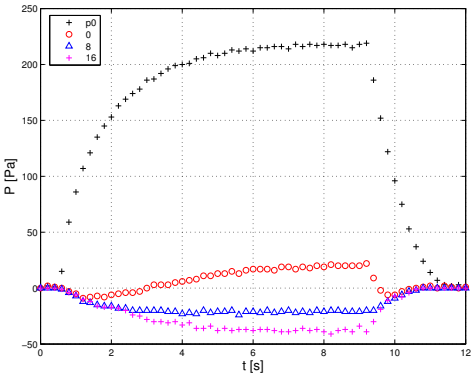

Figure 13: Measured pressures P(t) for the deformable replica for P_{in} set to 200 Pa for the upstream pressure (p_0) and for the pressure taps at the positions indicated in Figure 8(b) to the middle of the metal cylinder 0 (○), 8 (△) and 16 (+) mm thereafter labelled 0, 8 and 16 respectively.

ure 8(b). In absence of flow the minimum constriction coincides with the position of the

pressure tap p_1 at the centre of the metal support in Figure 8(b). The positions in Figure 13 are labelled with respect to their distance (in mm) to this reference point p_1 labelled 0. Increasing the upstream pressure p_0 results in negative pressures at all pressure taps, i.e. at the support centre 0, 8 and 16 mm further downstream. Further increasing the pressure results in a further decrease 16 mm after the centre while at the centre a positive pressure is retrieved. Therefore the curves confirm the displacement of the minimum constriction in the flow direction prevailed in the dye experiment illustrated in Figure 10. The overall model prediction illustrated in Figure 12 agrees well with the experimental data. In all cases the error remains well below 20 % considered as the upper limit for worst case error. Replica reopening is observed in Figure 12(a) for experimental data 1. This behaviour can not be predicted by the current model proposed in [16, 18] due to the assumption of quasi-steadiness. Reopening is associated with the onset of instabilities retrieved in e.g. snoring. This illustrates the mentioned relationship between OSA and snoring but shows at the same time the difference between the two phenomena. The flow limitation due to the wall displacement characterising the collapse is for the examples showed in Figure 12 quantified in [16, 18] and yield 49.9 and 69.6 %, respectively. The percentages of flow limitation are comparable to 'in-vivo' order of magnitudes of about 50 % in case of hypopnea. So both the theoretical as the experimental model are suitable to study at partial collapse and in particular the presented experimental model is therefore a valuable alternative to the classical Starling resistor experiment. The theoretical model is not capable to predict total collapse since among others a collision model is not taken into account. The contact during the collision influences e.g. the onset of instabilities to a large extent as shown in [109].
A first preliminary qualitative 'in-vivo' validation of the theoretical model is presented in [17]. Pre- and post-operative (maxillomandibular surgery) geometries are extracted from sagittal radiographies obtained on two patients suffering from obstructive sleep apnea. Results are detailed and extensively discussed and are in good agreement with clinical data. So the clinical validation is encouraging, but should be extended to a larger number of subjects. Moreover considering 'in-vivo' data multiple constriction sizes can be found. Therefore the study of the theoretical and experimental model should be continued and e.g. the downstream influence on an upstream constriction should be considered in further modelling. Nevertheless the proposed model provides a trade off between accuracy and simplicity resulting from motivated and thoroughly validated assumptions. The proposed approach seems to offer a workable tool for clinical applications in terms of computational load and at the same time to favour physical understanding since important flow phenomena are identified at the begin of the model design. Inclusion of second order effects in simplified models remains a challenging and fundamental task and is subject to current research as e.g. shown in [59] for the effect of asymmetry predisposing the experimentally found forward movement depicted in section 7.3.3.

9 Conclusion

Despite excellent research, the current state of the art considering the diagnosis, treatment and understanding of obstructive sleep apnea would benefit from improved physical understanding allowing to identify and quantify the principle phenomena involved. Since 'in-vivo' physiological observations are the result from highly complex fluid-structure-neural interactions 'in-vitro' experimental models are proposed in order to validate the problem formulation and to study the phenomena in a controllable and far simplified configurations neglecting neural control mechanisms. In case of physiological fluid-structure interactions as the obstructive sleep apnea syndrome the experimental model can be brought back to the study of collapsible tubes as in the classical Starling resistor experiment. Although the anatomical properties encountered in the upper airways exhibit an asymmetry in both geometry as mechanical properties which can not be attained by considering the Starling resistor. Therefore the current study proposes alternative experimental models with different complexity. Firstly a rigid replica is applied approximating a narrowed asymmetrical geometry. Secondly the asymmetry in mechanical properties of the surrounding structures is considered in addition to the geometrical asymmetry by partly replacing the rigid structure with a deformable portion. The deformable experimental model allows to reproduce both a hypopnea as an apnea event in case a suitable experimental setup is used. The setup should be capable to produce the required airflow, to impose the different parameters and to measure quantities of interest. Therefore the experimental model is, despite the severe simplifications, suitable to study fluid structure phenomena at the basis or at least largely involved in 'in-vivo' obstructive sleep apnea events. Variation from the Starling resistor seems hence possible and should be given a thought with respect to the study of e.g. obstructive sleep apnea.

Accounting for currently available standard computer capacity and limitations in solving the complete set of governing equations describing the fluid structure interaction in its full complexity the searched theoretical model strives to balance between simplicity and accuracy. Quantitative accuracy in the model outcome is a must considering medical applications while simplicity is obtained by accounting for first order phenomena revealing the nature of the problem and hence favouring understanding. Therefore a simplified flow model is applied. The underlying assumptions are based on 'in-vivo' observed characteristics and are thoroughly validated on a rigid experimental model. Next the flow model is integrated in a segregated fluid structure model in which the structure is approximated with a finite element model capable to model a partial collapse. Application of the theoretical model to the experimental deformable model matches well in terms of the predicted deformation and flow limitation. Furthermore encouraging results are obtained on 'in-vivo' data from pre- and postoperative sagittal radiographies. Nevertheless fundamental research efforts should be pursued firstly to identify, describe and incorporate major and minor effects in the theoretical model as among others wall contact during a complete collapse, flow reattachment and multiple constrictions and secondly to exploit the simplicity of the current model in an enlarged model of respiratory control to prospect the interweaving between central and

obstructive sleep apnea from a modeling point of view.

Acknowledgments

The authors would like to thank Pierre Chardon, Alexis Teulé, Vincent Pradel, Alice Perret, Nicolas Ruty, Samuel Paumard, Yves Garnier, Julien Cisonni, Freek van Uittert and Phillippe-Arnaud Plassard for their valuable contributions. The work is partly granted by the CNRS and the Rhône-Alpes region, France.

References

[1] M. Abbott, L. Donnelly, B. Dardzinski, S. Poe, B. Chini, and R. Amin. Obstructive sleep apnea: MR imaging volume segmentation analysis. *Radiology*, 232(3):889–895, 2004.

[2] M. Aittokallio, M. Gyllenberg, and O. Polo. A model of a snorer's upper airway. *Math. Biosc.*, 170:79–90, 2001.

[3] M. Aittokallio and O. Polo. Adjustment of the human respiratory system to increased upper airway resistance during sleep. a model of a snorer's upper airway. *Bulletin of Mathematical Biology*, 64:3–28, 2002.

[4] G. Allen, B. Shortall, T. Gemci, T. Corcoran, and N. Chigier. Computational simulations of airflow in an in-vitro model of the pediatric upper airways. *Transactions of the ASME*, 126:604–613, 2004.

[5] R. Arens, S. Sin, J. McDonough, J. Palmer, T. Dominguez, H. Meyer, D. Wootton, and A. Pack. Changes in upper airway size during tidal breathing in children with obstructive sleep apnea syndrome. *Am J Respir Crit Care Med*, 171(11):1298–1304, 2005.

[6] Y. Auregan and C. Depollier. Snoring: linear stability analysis and in vitro experiments. *J. Sound and Vibration*, 188(1):39–54, 1995.

[7] Y. Auregan and N. Meslier. Modelisation des apnees obstructives du sommeil. *C. R. Acad. Sci. Paris*, 316:1529–1534, 1993.

[8] I. Ayappa and D. Rapoport. The upper airway in sleep: physiology of the pharynx. *Sleep Medicine Reviews*, 7(1):9–33, 2003.

[9] T. Balint and A. Lucey. Instability of a cantilevered flexible plate in viscous channel flow. *J. of Fluids and Structures*, 20:893–912, 2005.

[10] C. Bertram and T. Pedley. A mathematical model of unsteady collapsible tube behaviour. *J. of Biomechanics*, 15(1):39–50, 1982.

[11] C. Bertram and J. Tscherry. The onset of flow-rate limitation and flow-induced oscillations in collapsible tubes. *J. of Fluids and Structures*, In press, 2006.

[12] R. Blevins. *Applied Fluid dynamics handbook*. Krieger publishing company, Malabar, 1992.

[13] S. Bridgman and K. Dunn. Surgery for obstructive sleep apnoea. *Cochrane Database Syst Rev*, 2:CD001004, 2002.

[14] R. Brower and A. Noordergraaf. Pressure-flow characteristics of collapsible tubes: A reconciliation of seemingly contradictory results. *Annals of biomedical engineering*, 1:333–355, 1973.

[15] C. Burwell, E. Robin, R. Whaley, and A. Bickelmann. Extreme obesity associated with an alveolar hypoventilation. a pickwickian syndrome. *Amer. J. Med.*, 21:811–817, 1956.

[16] F. Chouly. *Modélisation physique des voies aériennes supérieures pour le syndrome d'apnées obstructives du sommeil*. PhD thesis, 2005.

[17] F. Chouly, A. Van Hirtum, P.Y. Lagrée, J.R. Paoli, X. Pelorson, and Y. Payan. Simulation of the retroglossal fluid-structure interaction during obstructive sleep apnea. *Lecture Notes in Computer Science*, 4072:48–57, 2006.

[18] F. Chouly, A. Van Hirtum, P.Y. Lagrée, X. Pelorson, and Y. Payan. An attempt to model fluid-structure interaction during obstructive sleep apnea syndrome: numerical simulations and validation. *J. of Fluids and Structures*, In revision.

[19] M. Ciscar, G. Juan, V. Martinez, M. Ramon, T. Lloret, J. Minguez, M. Armengot, J. Marin, J. Magnetic resonance imaging of the pharynx in OSA patients Basterra, and 2001; 17(1): 79 86. healthy subjects Eur. Respir. J., January 1. Magnetic resonance imaging of the pharynx in OSA patients and healthy subjects. *Eur. Respir. J.*, 17(1):79–86, 2001.

[20] P. Collard, P. Rombaux, and D. Rodenstein. Why should we enlarge the pharynx in obstructive sleep apnea. *Sleep*, 19(9):85–87, 1996.

[21] R. Condos, R. Norman, I. Krishnasamy, N. Peduzzi, R. Goldring, and D. Rapoport. Flow limitation as a non-invasive assessment of residual upper-airway resistance during continuous positive airway pressure therapy of obstructive sleep apnea. *Am J Respir Crit Care Med*, 150(2):475–480, 1994.

[22] W. Conrad. Pressure-flow relationships in collapsible tubes. *IEEE Trans BioMed Eng*, 16:284–295, 1969.

[23] W. Conway, D. Lyle, D. Magilligan, S. Fujita, F. Zorick, and T. Roth. Adverse effects of tracheostomy for sleep apnea. *JAMA*, 246:347–350, 1987.

[24] J. Cullen, J. Gilbert, and M. Campbell. Brass instruments: linear stability analysis and experiments with an artificial mouth. *Acta Acustica*, 86:704–724, 2000.

[25] J. Cummiskey, T. Williams, P. Krumpe, and C. Guilleminault. The detection and quantification of sleep apnea by tracheal sound recordings. *Am Rev Respir Dis*, 126:221–224, 1982.

[26] R. Davies and J. Stradling. The relationship between neck circumference radiographic pharyngeal anatomy, and the obstructive sleep apnoea syndrome. *Eur. Respir. J.*, 3:509–514, 1990.

[27] H. Demin, Y. Jingying, W. Jun, Y. Qingwen, and W. Jiangyong. Determining the site of airway obstruction in obstructive sleep apnea with airway pressure measurements during sleep. *Laryngoscope*, 112:2081–2085, 2002.

[28] M. Deverge, X. Pelorson, C. Vilain, P. Lagree, F. Chentouf, J. Willems, and A. Hirschberg. Influence of collision on the flow through in-vitro rigid models of the vocal folds. *J. Acoust. Soc. Am.*, 114(6):1–9, 2003.

[29] N. Douglas. Home diagnosis of the obstructive sleep apnoea/hyopnoea syndrome. *Sleep Medicine Reviews*, 7(1):53–59, 2003.

[30] J. Drazen. Sleep apnea syndrome. *New England J. of Medicine*, 6:346–390, 2002.

[31] L. Findley, M. Unverzagt, and P. Suratt. Automobile accidents involving patients with obstructive sleep apnea. *Am Rev Respir Dis*, 138:337–340, 1988.

[32] A. Fishman, P. Macklem, J. Mead, and S. Geiger. *The respiratory system. In Handbook of physiology*. Am. Phys. Soc., Maryland, 1986.

[33] W. Flemons. Obstructive sleep apnea. *New England J. of Medicine*, 347(7):498–504, 2002.

[34] W. Flemons and M. Reimer. Measurement properties of the calgary sleep apnea quality of life index. *Am. J. Respir. Crit. Care Med.*, 165:159–164, 2002.

[35] R. Fodil, C. Ribreau, B. Louis, F. Lofaso, and D. Isabey. Interaction between steady flow and individualised compliant segments: application to upper airways. *Medical & Biological Engineering and Computing*, 35(6):638–648, 1997.

[36] R. Fogel, A. Malhotra, and D. White. Pathophysiology of obstructive sleep apnoea/hypopnoea syndrome. *Thorax*, 59(2):159–163, 2004.

[37] S. Gallet, P. Meunier, and G. Spedding. Empirical scaling of antisymmetric stratified wakes. *J. of Fluid Mechanics*, 22:941–947, 2006.

[38] N. Gavriely and O. Jensen. Theory and measurements of snores. *J. of Appl. Physiol.*, 74(6):2828–2837, 1993.

[39] D. Gottlieb. Can sleep apnea be treated without modifying anatomy ? *New England J. of Medicine*, 353:2604–2606, 2005.

[40] G. Gould, K. Whyte, G. Rhind, M. Airlie, J. Catterall, C. Shapiro, and N. Douglas. The sleep hypopnea syndrome. *Am Rev Respir Dis*, 137:895–898, 1988.

[41] J. Grotberg and O. Jensen. Biofluid mechanics in flexible tubes. *Annu. Rev. Fluid Mech.*, 36:121–147, 2004.

[42] P. Gumery, H. Roux-Buisson, S. Meignen, F. Comyn, M. Dematteis, B. Wuyam, J. Pepin, and P. Levy. An adaptive detector of genioglossus EMG reflex using berkner transform for time latency measurement in OSA pathophysiological studies. *IEEE Trans BioMed Eng*, 52(8):1382–1389, 2005.

[43] M. Heil and O. Jensen. *Flows in deformable tubes and channels – Theoretical models and biological applications*, chapter Flow in Collapsible Tubes and Past Other Highly Compliant Boundaries, pages 15–50. Kluwer, Dordrecht, The Netherlands, 2003.

[44] K. Henke. Upper airway muscle activity and upper airway resistance in young adults during sleep. *J. of Appl. Physiol.*, 84(2):486–491, 1998.

[45] G.C.J. Hofmans, G. Groot, M. Ranucci, and G. Graziani. Unsteady flow through in-vitro models of the glottis. *J. Acoust. Soc. Am.*, 113(3):1658–1675, 2003.

[46] R. Horner, Innes J., M. Morell, S. Shea, and A. Guz. The effect of sleep on reflex genioglossus muscle activation by stimuli of negative airway pressure in humans. *J. Physiol.*, 476(1):141–151, 1994.

[47] L. Huang. Mechanical modeling of palatal snoring. *J. Acoust. Soc. Am.*, 97:3642–3648, 1995.

[48] L. Huang and J. Ffowcs Williams. Neuromechanical interaction in human snoring and upper airway obstruction. *J. of Appl. Physiol.*, pages 1759–1763, 1999.

[49] Y. Huang, A. Malhotra, and D. White. Computational simulation of human upper airway collapse using a pressure-/state-dependent model of genioglossal muscle contraction under laminar flow conditions. *J. of Appl. Physiol.*, 99:1138–1148, 2005.

[50] Y. Huang, D. White, and A. Malhotra. The impact of anatomic manipulations on pharyngeal collapse: results from a computational model of the normal human upper airway. *Chest*, 128(3):1324–1330, 2005.

[51] F. Huarte, P. Bearman, and J. Chaplin. On the force distribution along the axis of a flexible circular cylinder undergoing multi-mode vortex-induced vibrations. *J. of Fluid Mechanics*, 22:897–903, 2006.

[52] D. Hui, D. Choy, F. Ko, T. Li, and C. Lai. Obstructive sleep apnoea syndrome: treatment update. *Medical practice*, 6(2):209–217, 2000.

[53] S. Isono, D. Morrison, H. Launois, T. Feroah, W. Whitelaw, and J. Remmers. Static mechanics of the velopharynx of patients with obstructive sleep apnea. *J. of Appl. Physiol.*, 75:148–154, 1993.

[54] S. Isono, J. Remmers, A. Tanaka, Y. Sho, J. Sato, and T. Nishino. Anatomy of pharynx in patients with obstructive sleep apnea and in normal subjects. *J. of Appl. Physiol.*, 82(4):1319–1326, 2001.

[55] A. Katz, Y. Chen, and A. Moreno. Flow through a collapsible tube: experimental analysis and mathematical model. *Biophys J.*, 9:1261–1279, 1969.

[56] E. King, C. O'Donnell, P. Smith, and A. Schwartz. A model of obstructive sleep apnea in normal humans role of the upper airway. *Am. J. Respir. Crit. Care Med.*, 161(6):1979–1984, 2000.

[57] J. Krieger, C. Petiau, E. Sforza, T. Weiss, A. Thibault, and A. Bazin. Resisteur de Starling et stabilite du couple sommeil-ventilation. *Neurophysiologie Clinique*, 28:493–506, 1998.

[58] P. Lagrée and S. Lorthois. The RNS/Prandtl equations and their link with other asymptotic descriptions. Application to the computation of the maximum value of the wall shear stress in a pipe. *Int. J. Eng Sci.*, 43:352–378, 2005.

[59] P.Y. Lagrée, A. Van Hirtum, and X. Pelorson. Asymmetrical effects in a 2D stenosis. *European Journal of Mechanics B/Fluids*, In press.

[60] R. Lambert and T. Wilson. Flow limitation in a collapsible tube. *J. of Appl. Physiol.*, 33(1):150–153, 1972.

[61] A. Laneville. On vortex-induced vibrations of cylinders describing X-Y trajectories. *J. of Fluid Mechanics*, 22:773–782, 2006.

[62] J. Leiter. Upper airway shape: Is it important in the pathogenesis of obstructive sleep apnea? *Am. J. Respir. Crit. Care Med.*, 153(3):894–898, 1996.

[63] D.E Leith, J.P. Butler, S.L. Sneddon, and J.D. Brain. *Cough in Handbook of physiology III*. American physiology society, Maryland, 1986.

[64] J. Leontini, M. Thompson, and K. Hourigan. The beginning of branching behaviour of vortex-induced vibration during two-dimensional flow. *J. of Fluid Mechanics*, 22:857–864, 2006.

[65] T. Leweke, M. Thompson, and K. Hourigan. Instability of the flow around and impacting sphere. *J. of Fluid Mechanics*, 22:961–971, 2006.

[66] J. Lindman and C. Morgan. Obstructive sleep apnea syndrome. *eMedecine*, 2005.

[67] A. Lipton and D. Gozal. Treatment of obstructive sleep apnea in children : do we really know how ? *Sleep Medicine Reviews*, 7(1):61–80, 2003.

[68] A. Lipton and D. Gozal. Obstructive sleep apnea syndrome. *eMedecine*, 2004.

[69] Z. Liu, X. Luo, H. Lee, and C. Lu. Snoring source identification and snoring noise prediction. *J. of Biomechanics*, In press.

[70] A. Lucey and T. Balint. Instability of an elastic cantilevered plate in channel flow: An analogue mechanical model for snoring and sleep apnoea. In *Proc. World Congress on Medical Physics and Biomedical Engineering*, 2003.

[71] C. Lyon, J. Scott, and C. Wang. Flow through collapsible tubes at low reynolds numbers. applicability of the waterfall model. *Circ Res*, 47(19):68–73, 1980.

[72] A. Malhotra, Y. Huang, R. Fogel, G. Pillar, J. Edwards, R. Kikinis, S. Loring, and D. White. The male predisposition to pharyngeal collapse. importance of airway length. *Am J Respir Crit Care Med*, 166:1388–1395, 2002.

[73] A. Malhotra and D. White. Obstructive sleep apnoea. *The Lancet*, 360:237–245, 2002.

[74] K. Mansour, J. Rowley, A. Meshenish, M. Shkoukani, and M. Badr. A mathematical model to detect inspiratory flow limitation during sleep. *J. of Appl. Physiol.*, 93:1084–1092, 2002.

[75] A. Marzo, X. Luo, and C. Bertram. Three-dimensional collapse and steady flow in thick-walled flexible tubes. *J. of Fluids and Structures*, 20(6):817–835, 2005.

[76] Y. Matsuzaki and Y. Fung. On separation of a divergent flow at moderate Reynolds numbers. *ASME J. Appl. Mech.*, 43:227–231, 1976.

[77] P. Mayer, J.L. Pepin, G. Bettega, D. Veale, G. Ferreti, C. Deschaux, and P. Levy. Relationship between body mass index, age and upper airway measurements in snorers and sleep apnea patients. *Eur. Respir. J.*, 9:1801–1809, 1996.

[78] W. McNicholas. Sleep apnoea syndrome today: much done, more to do. *Sleep Medicine Reviews*, 7(1):1087–1093, 2003.

[79] M. Morrell, Y. Arabi, B. Zahn, and M. Badr. Progressive retropalatal narrowing preceding obstructive apnea. *Am J Respir Crit Care Med*, 158:1974–1981, 1998.

[80] A. Pack. *Sleep Apnea- Pathogenesis, Diagnosis, and Treatment*. Lung Biologie in Health and disease. Marcel Dekker, Basel, Switzerland, 2002.

[81] A. Pack. Advances in sleep-disordered breathing. *Am. J. Respir. Crit. Care Med.*, 173(1):7–15, 2006.

[82] M. Paidoussis. Wave propagation in physiological collapsible tubes and a proposal for a Shapiro number. *J. of Fluid Mechanics*, 22:721–725, 2006.

[83] Y. Payan, M. Chabanas, X. Pelorson, C. Vilain, P. Levy, V. Luboz, and P. Perrier. Biomechanical models to simulate consequences of maxillofacial surgery. *C. R. Biologies*, 325:407–417, 2002.

[84] T. Pedley and X. Luo. Modelling flow and oscillations in collapsible tubes. *J. of Theoret. Comp. Fluid Dynamics*, 10:227–294, 1998.

[85] X. Pelorson, A. Hirschberg, R. Van Hasselt, A. Wijnands, and Y. Auregan. Theoretical and experimental study of quasisteady-flow separation within the glottis during phonation. application to a modified two-mass model. *J. Acoust. Soc. Am.*, 96(6):3416–3431, 1994.

[86] T. Penzel, J. McNames, P. de Chazal, B. Raymond, A. Murray, and G. Moody. Systematic comparison of different algorithms for apnoea detection based on electrocardiogram recordings. *Medical & Biological Engineering & Computing*, 40:402–407, 2002.

[87] P. Peppard, T. Young, M. Palta, and J. Skatrud. Prospective study of the association between sleep-disordered breathing and hypertension. *New England J. of Medicine*, 342(19):1378–1374, 2000.

[88] J. Perez-Padilla, E. Slawinski, L. Difrancesco, R. Feige, J. Remmers, and W. Whitelaw. Characteristics of the snoring noise in patients with and without occlusive sleep apnoea. *Am Rev Respir Dis*, 147:635–644, 1993.

[89] A. Philip. On the nature of sleep. *Phil. Trans. R. Soc. Lond. A*, 123:73–87, 1833.

[90] E. Phillipson and J. Remmers. Indications and standards for cardiopulmonary sleep studies. *Am Rev Respir Dis*, 139:559–568, 1989.

[91] A. Rama, S. Tekwant, and C. Kushida. Sites of obstruction in obstructive sleep apnea. *Chest*, 122(4):1139–1147, 2002.

[92] S. Redmond and C. Heneghan. Cardiorespiratory-based sleep staging in subjects with obstructive sleep apnea. *IEEE transactions on vizualization and computer graphics*, 53(3):485–496, 2006.

[93] J. Remmers, W. deGroot, E. Sauerland, and A. Anch. Pathogenesis of upper airway occlusion during sleep. *J. of Appl. Physiol.*, 44:931–938, 1978.

[94] N. Ruty, X. Pelorson, Annemie Van Hirtum, I. Lopez, and A. Hirschberg. An in-vitro setup to test the relevance and the accuracy of low-order vocal folds models. *J. Acoust. Soc. Am.*, In review.

[95] N. Ruty, A. Van Hirtum, X. Pelorson, I. Lopez, and A. Hirschberg. A mechanical experimental setup to simulate vocal folds vibrations. preliminary results. *ZAS papers in Linguistics*, 40:161–175, 2005.

[96] H. Schlichting and K. Gersten. *Boundary layer theory*. Springer Verlag, Berlin, 2000.

[97] W. Schmidt-Nowara, A. Lowe, L. Wiegand, R. Cartwright, F. Perez-Guerra, and S. Menn. Oral appliances treatment of snoring and obstructive review. *Sleep*, 18(6):501–510, 1995.

[98] R. Schwab, M. Pasirstein, R. Pierson, A. Mackley, R. Hachadoorian, R. Arens, G. Maislin, and A. Pack. Identification of upper airway anatomic risk factors for obstructive sleep apnea with volumetric magnetic resonance imaging. *Am. J. Respir. Crit. Care Med.*, 168:522–530, 2003.

[99] R.J. Schwab, W.B. Gefter, E.A. Hoffman, K.B. Gupta, and A.I. Pack. Dynamic upper airway imaging during awake respiration in normal subjects and patients with sleep disordered breathing. *Am J Respir Crit Care Med*, 148:1385–1400, 1990.

[100] A. Schwartz, J. Kirkness, and P. Smith. Extraluminal tissue pressure: what does it mean? *J. of Appl. Physiol.*, 100(1):5–6, 2006.

[101] A. Sher, K. Schechtman, and J. Piccirillo. The efficacy of surgical modifications of the upper airway in adults with obstructive sleep apnea syndrome. *Sleep*, 19:156–177, 1996.

[102] B. Shome, L. Wang, M. Santare, A. Prasad, A. Szeri, and D. Roberts. Modeling of airflow in the pharynx with application to sleep apnea. *J. of Biomechanical Engineering*, 120:416–422, 1998.

[103] P. Smith and A. Gill. Question: is surgery effective for reducing symptoms in adults with obstructive sleep apnea. *J. Family Practi*, 50:17–18, 2001.

[104] P. Smith, R. Wise, A. Gold, A. Schwartz, and S. Permutt. Upper airway pressure-flow relationships in obstructive sleep apnea. *J. of Appl. Physiol.*, 64:789–795, 1988.

[105] H. Steltner, R. Staats, J. Timmer, M. Vogel, J. Guttmann, H. Matthys, and J. Virchow. Diagnosis of sleep apnea by automatic analysis of nasal pressure and forced oscillation impedance. *Am J Respir Crit Care Med*, 165:940–944, 2002.

[106] P. Strollo and R. Rogers. Obstructive sleep apnea. *New England J. of Medicine*, 334:99–104, 1996.

[107] R. Tamisier, J. Pepin, B. Wuyam, C. Deschaux, and P. Levy. Expiratory changes in pressure: flow ratio during sleep in patients with sleep-disordered breathing. *Sleep*, 27(2):240–248, 2004.

[108] J. Teran-Santos, A. Jiminez-Gomez, and J. Cordero-Guevara. The association between sleep apnea and the risk of traffic accidents. *New England J. of Medicine*, 340(11):847–851, 1999.

[109] A. Van Hirtum, J. Cisonni, N. Ruty, X. Pelorson, I. Lopez, and F. van Uittert. Experimental validation of some issues in lip and vocal fold physical models. *Acta Acustica*, Accepted.

[110] A. Van Hirtum, X. Pelorson, and P.Y. Lagrée. In vitro validation of some flow assumptions for the prediction of the pressure distribution during obstructive sleep apnoea. *Medical & Biological Engineering & Computing*, 43:162–171, 2005.

[111] B. Woodson. Expiratory pharyngeal airway obstruction during sleep: A multiple element model. *Laryngoscope*, 113:1450–1459, 2003.

[112] D. Wootton, A. Guez, P. Vaidyanathan, D. McDonough, J. Udupa, and R. Arens. Image-based modeling of upper airway flow in children with obstructive sleep apnea. In *Proc. Summer Bioengineering Conference*, page 2, 2003.

[113] C. Xu. *Computational Mechanics Models for studying the pathogenesis of Obstructive Sleep Apnea*. PhD thesis, Drexel University, 2005.

[114] C. Xu, S. Sin, J. McDonough, J. Udupa, A. Guez, R. Arens, and D. Wootton. Computational fluid dynamics modeling of the upper airway of children with obstructive sleep apnea syndrome in steady flow. *J. of Biomechanics*, 39(11):2043–2054, 2006.

[115] H. Yaggi, J. Concato, W. Kernan, J. Lichtman, L. Brass, and V. Mohsenin. Obstructive sleep apnea as a risk factor for stroke and death. *New England J. of Medicine*, 353:2034–2041, 2005.

[116] Y. Yamashiro and M. Kryger. Why should sleep apnea be diagnosed and treated ? *Clin Pulm Med*, 1:250–259, 1994.

[117] T. Young, M. Palta, J. Dempsey, J. Skatrud, S. Weber, and S. Badr. The occurrence of sleep-disordered breathing among middle-aged adults. *New England J. of Medicine*, 17(328):1230–1235, 1993.